Some numerical studies of exotic shock wave behavior

Some numerical studies of exotic shock wave behavior

Jason W. Bates[a] and David C. Montgomery
Department of Physics & Astronomy, Dartmouth College, Hanover, New Hampshire 03755

(Received 2 June 1998; accepted 21 October 1998)

For shock waves propagating in materials with nonideal equations of state, a variety of nonstandard phenomena can occur. Here, we present numerical studies of two such exotic shock effects: (i) ''anomalous'' behavior, in the terminology of Zel'dovich and Raizer; and (ii) a search for ''acoustic emission instabilities.'' The motivation is in part the possibility of such phenomena in the implosion of inertial confinement fusion (ICF) pellet materials, whose equations of state are currently far from well known. In shock wave theory, anomalous materials are those whose isentropes have regions of negative curvature (in the plane of pressure versus specific volume) through which the shock adiabatic passes. The existence of such regions is significant because they can interfere with the steepening of compressive pulses into shocks, lead to the formation of rarefactive shock waves, and even cause shocks to ''split.'' A van der Waals fluid with a large heat capacity is one example of a material possessing such anomalous properties. Acoustic emission instability—the second exotic shock mechanism considered—may occur when the slope of the shock adiabatic lies below a critical value. In this phenomenon, perturbations of a two-dimensional planar shock front can render it unstable, and lead to the downstream emission of acoustic waves. In addition to the van der Waals fluid, an equilibrium dissociation model for strong shocks in diatomic hydrogen is shown to fulfill the theoretical criteria for this instability, but its numerical verification has been hard to achieve, suggesting that further study is needed. Both classes of phenomena may be expected to play a role in ICF compression scenarios. © *1999 American Institute of Physics.* [S1070-6631(99)01402-6]

I. INTRODUCTION

In some inertial confinement fusion (ICF) schemes, it is intended to compress deuterium–tritium (DT) pellets by one or more imploding shock compressions, to densities as much as 1000 times greater than solid DT values, and to temperatures of several keV. The compressions will lead through regimes where the equations of state (EOS) of hydrogen isotopes are still imperfectly known and very difficult to measure, e.g., see Refs. 1–3. In Refs. 2 and 3, and more recently in Ref. 4, there is evidence that the shock Hugoniot may pass through regions associated with phase transitions where highly nonideal equations of state might be involved. It is possible that such phenomena as ''anomalous'' shock wave behavior[5–7] or ''acoustic emission instabilities'' (also known as ''transverse wave instabilities'')[8–12] might occur, and if they did, could be important considerations with regard to the efficiency of the compression. Our purpose in this paper is to report some hydrodynamical simulations of such shock peculiarities and to suggest some possible consequences of them for ICF target compression.

In shock wave theory,[5,12] a central role is played by the ''shock Hugoniot'' or ''shock adiabatic'' curve in the (V,p) plane, where V is the volume per unit mass of the material (specific volume), and p is the pressure. The shock adiabatic is the locus of all those values of V and p which may be connected by a single shock, starting from initial (''unshocked'' or ''upstream'') values of V and p, and leading to a pair of ''shocked'' or ''downstream'' values. Both the initial and final states of the material are assumed to be in local thermodynamic equilibrium and are separated by a moving shock discontinuity across which mass, momentum, and energy are conserved.

A key point in the standard development is the demonstration that shocks can only be compressive and not rarefactive under normal conditions,[5] using the inequality $(\partial^2 p/\partial V^2)_s > 0$, where the derivatives are computed holding the specific entropy s fixed. This inequality can be shown to be equivalent to $c'(\rho) > -c(\rho)/\rho$, where $c(\rho)$ is the adiabatic sound speed and $\rho = 1/V$ is the mass density. This inequality is valid for the vast majority of materials in which shocks are typically launched. However, *it is not a thermodynamic requirement*, and it has long been noted[5–7] that there exist regions of phase space in which the inequality is reversed. For such ''anomalous'' substances, rarefactive shocks are thermodynamically possible in some regions and compressive ones are not. Ivanov and Novikov[13] were apparently the first to document clear experimental evidence of this effect in iron and steel near a polymorphic phase transition. In later years, Thompson and co-workers[14–17] provided compelling demonstrations of anomalous behavior in a variety of other materials.

The sign of the quantity $(\partial^2 p/\partial V^2)_s$ is also an important consideration with regard to the *stability* of shock waves. For a two-dimensional compressive shock whose adiabatic passes *through* an anomalous region of the (V,p) plane, downstream perturbations of the flow field may stimulate the

[a]Present address: Hydrodynamic Methods Group (X-HM), Applied Theoretical and Computational Physics Division, MS D413, Los Alamos National Laboratory, Los Alamos, New Mexico 87545.

shock to ''split'' into two other shocks, which are then stable, but possess different amplitudes and propagation velocities.[18] The splitting process is, of course, an irreversible one, and is evidently accompanied by the emission of an acoustic wave that moves away from the shock front in the downstream direction.[11,19]

One signature of an anomalous region for a material in the (V,p) plane is a shock adiabatic which is locally concave downward rather than upward. Experimental techniques exist for measuring shock adiabatics[4,7] even when the measurement does not permit the extraction of the full EOS from which the shock adiabatic could be inferred theoretically. One popular way of exhibiting shock adiabatics is by plotting the logarithm of the pressure as a function of the mass density for the downstream region. In such a plot, a region of negative slope may have associated with it an anomalous region for the material at any place where the curvature of the adiabatic is also concave downward. Though the calculation of the EOS for hydrogen isotopes at solid densities remains provisional and difficult, anomalous regions may be suggested, for example, by Fig. 16 of More *et al.*[2] and by Fig. 4(b) of DaSilva *et al.*[4]

Some of these Hugoniot data also suggest that hydrogen isotopes at high temperatures may be susceptible to another exotic shock wave mechanism known as acoustic emission. This phenomenon is a special type of instability in which deformations to the planarity of a compressive shock front are stationary and result in the enhancement of acoustic noise behind the shock.[20] It should be pointed out that this class of unstable shock-wave activity is distinct from so-called ''corrugation instabilities,'' in which perturbations to the front are predicted to grow with time.[8,12,21,22]

Using a linearized normal mode analysis, Kontorovich[9] derived the criteria for acoustic emission in the form of inequalities involving the parameter

$$h = j^2 \left(\frac{dV}{dp} \right)_H , \tag{1}$$

where $j^2 = (p_2 - p_1)/(V_1 - V_2)$ is the square of the mass flux density across the shock, and subscripts ''1'' and ''2'' denote upstream and downstream values, respectively; the derivative is taken along the shock adiabatic (Hugoniot) and evaluated at the downstream state. The condition for acoustic emission to occur can be stated as[9,11,12]

$$h_c < h < 1 + 2v_2/c_2 , \tag{2}$$

where

$$h_c = \frac{1 - v_2^2/c_2^2 - v_1 v_2/c_2^2}{1 - v_2^2/c_2^2 + v_1 v_2/c_2^2} . \tag{3}$$

Here, v is the fluid velocity in the frame of reference in which the shock is stationary. Equation (2) can be satisfied on some shock adiabatics having $(dp/dV)_H > 0$. However, because the lower limit h_c may be negative, it is also possible for instabilities of this type to arise on some sections of ordinary-shaped adiabatics with $(dp/dV)_H < 0$ everywhere.[12]

Fowles[10] obtained the instability condition in Eq. (2) by determining when the reflection coefficient of oblique acoustic waves (incident on the downstream face of the shock) becomes infinite. This implies that infinitesimal downstream perturbations to the flow can cause finite disturbances at the surface of discontinuity. Said another way, acoustic waves can be generated spontaneously at the shock front—thus rendering it unstable—whenever the inequalities in Eq. (2) are satisfied.

Experimental results reported by Thompson *et al.*[17] show evidence of this class of instabilities in shocks traveling through fluids with large heat capacities and in the vicinity of a phase transition. In addition, Mond and Rutkevich[23] have shown that instabilities of this type are likely to occur in inert gases through which strong ionizing shocks are passing. Their theoretical predictions seem to be in good agreement with the experimental shock-tube data presented by Griffiths, Sandeman, and Hornung,[24] and Glass and Liu,[25] for the case of argon gas.

In the following sections, we present numerical simulations of both anomalous behavior and a search for acoustic emission instabilities in shock waves. We begin in Sec. II by employing a van der Waals EOS with a large heat capacity as a tractable example of an anomalous fluid. Implications of anomalous behavior for shock propagation are investigated by studying numerically the results of one-dimensional hydrodynamical simulations of shock tubes. Ignoring the effects of viscosity and thermal conductivity, we use the ''flux corrected transport'' (FCT) method[26–28] to solve the nonlinear partial differential equations involved, i.e., the Euler equations. In a second series of runs, piston-launched compressive pulses are used to explore the dynamical formation of shock fronts from smooth initial data. This is done to gain confidence that the FCT technique is well adapted for studying shocks in media with anomalous (as well as more standard) equations of state. The topic of instabilities in two-dimensional shock waves is treated in Sec. III, where we show simulations for two different equations of state. For our first EOS, we again consider the van der Waals fluid near the known anomalous region, and an instability of the shock front results in a shock splitting. The second EOS used is perhaps of greater relevance to ICF research, and is based on a simple dissociation model of diatomic hydrogen. The results are somewhat unexpected, in that though the criteria for acoustic emission seem to be satisfied, we cannot say convincingly that any numerical evidence of instability has been observed in the simulations. Finally in Sec. IV, we summarize our findings and outline some suggestions for future research.

II. ANOMALOUS VAN DER WAALS FLUID BEHAVIOR

Anomalous behavior, in the sense of Zel'dovich and Raizer,[5] is not characteristic of ideal gases. Typically, it has been associated with the presence of nearby phase transitions in which particle interactions become significant in the energy budget. Any sudden increase of the adiabatic compressibility with density (and thereby, a sudden decrease in sound speed) may lead to anomalous behavior, and may occur in fluids or solids. Perhaps the simplest example of a material that exhibits such behavior arises in a van der Waals fluid,[5,29]

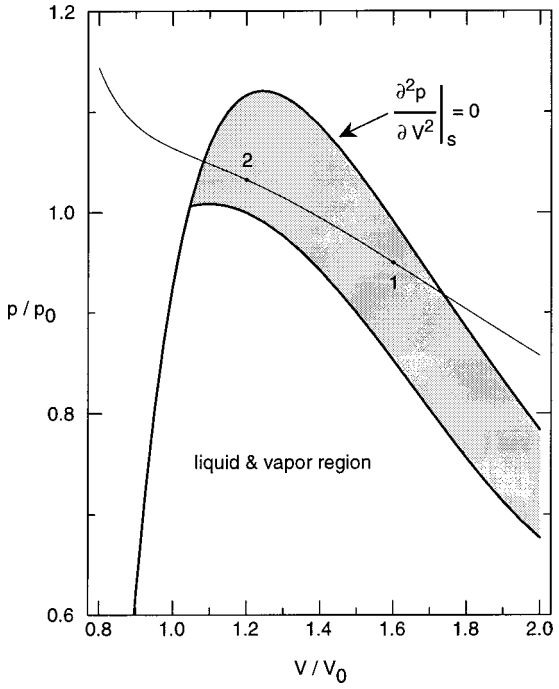

FIG. 1. Shock adiabatic through the one-phase anomalous region (shaded) of the (V,p) plane for a van der Waals fluid with $\mu c_V/R=80$. Initial and final states are $(V_1,p_1)=(1.6V_0,0.95p_0)$ and $(V_2,p_2)=(1.2V_0,1.03p_0)$, respectively. The critical point occurs at $V/V_0=1$ and $p/p_0=1$. The curve at the bottom of the shaded region denotes the boundary of the two-phase coexistence region.

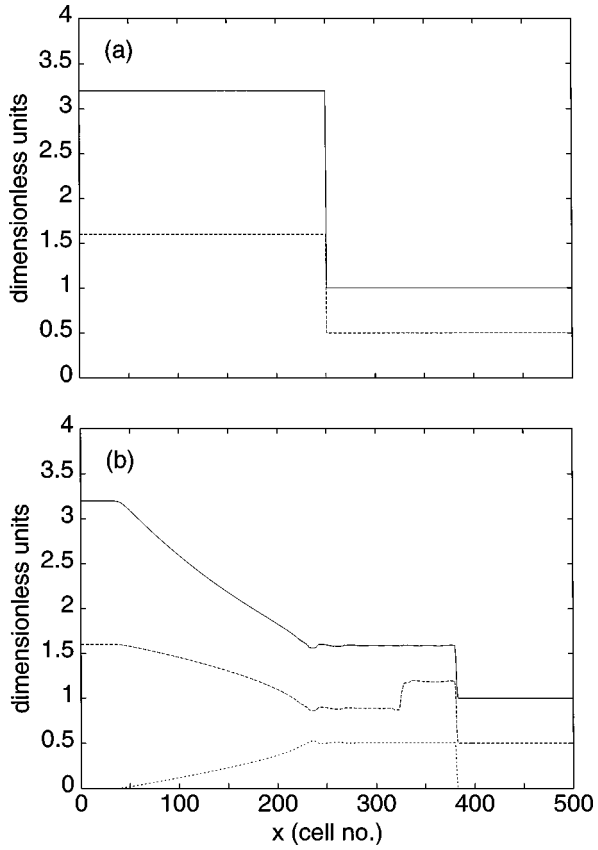

FIG. 2. One-dimensional shock-tube simulation of a van der Waals fluid in a nonanomalous region of the (V,p) plane, with $(V_1,p_1)=(2V_0,p_0)$, $(V_2,p_2)=(0.63V_0,3.2p_0)$, and $\mu c_V/R=80$, where $V_0=3b$ and $p_0=a/27b^2$. Profiles of pressure (solid line), density (dashed line), and velocity (dotted line) are shown at (a) $t=0$; and (b) $t=150$. A shock wave, clearly visible at $x\simeq 380$ in (b), travels to the right, while a rarefactive wave moves to the left. A contact discontinuity lies between.

just to the right of the critical point and outside the two-phase region in the (V,p) plane. Here, we will use a van der Waals EOS to illustrate dynamical consequences which result when it is attempted to launch shocks in anomalous media. Similar results may be expected any time the attractive forces between molecules begin to be strongly felt.

The pressure–volume relationship for a van der Waals fluid is well known:

$$(p+a/V^2)(V-b)=NkT, \tag{4}$$

where N is the number of molecules per unit mass, k is Boltzmann's constant, and T is the temperature. The constant a represents the effect of long-range attractive intermolecular forces, and the constant b represents the finite volume occupied by the molecules themselves. The ideal gas limit follows from setting a and b equal to zero. Supplementing Eq. (4) is the expression for the entropy increment ds,

$$Tds=d\varepsilon+pdV=c_V dT+\left(p+\frac{a}{V^2}\right)dV, \tag{5}$$

where ε is the internal energy per unit mass. For simplicity, we shall assume that the specific heat per unit mass at constant volume, c_V, is independent of temperature and equal to a constant, though this is not a consequence of Eq. (4).

For this van der Waals fluid, it is possible to express algebraically the entropy s and the energy ε as functions of V and p. The Rankine–Hugoniot relations[5,12] can then be used to construct the shock adiabatics, as well as the ''Poisson adiabatics'' or isentropes. In Fig. 1, we display a typical shock adiabatic which passes through an anomalous region (shaded). In creating this figure, the specific heat at constant volume was chosen to have a value $c_V=80R/\mu$, where R is the universal gas constant, and μ is the molecular weight of the fluid. This assumption amounts to considering many internal molecular degrees of freedom. The specific volumes and pressures in the plot are normalized to the reference values $V_0\equiv 3b$ and $p_0\equiv a/27b^2$, respectively. Other features of Fig. 1 will be explained later.

In order to study the effect of anomalous fluid properties on shock wave formation and compression, we have employed a gas-dynamical numerical code of the ''flux-corrected transport'' (FCT) variety.[26–28] The code involves inviscid one-dimensional equations of continuity, momentum, and energy, supplemented by an EOS given in our case by Eqs. (4) and (5). When shocks form from compressive pulses, the FCT code propagates them stably and according to the conservation laws, but does not address microscopic dissipative processes or issues of irreversibility.

Perhaps the simplest numerical example in which anomalous behavior is evident is in the simulation of a one-dimensional shock tube filled with a van der Waals fluid. Figures 2(a, b) and 3(a, b) show the results of using a FCT algorithm to model such a system. At time $t=0$, a ''dia-

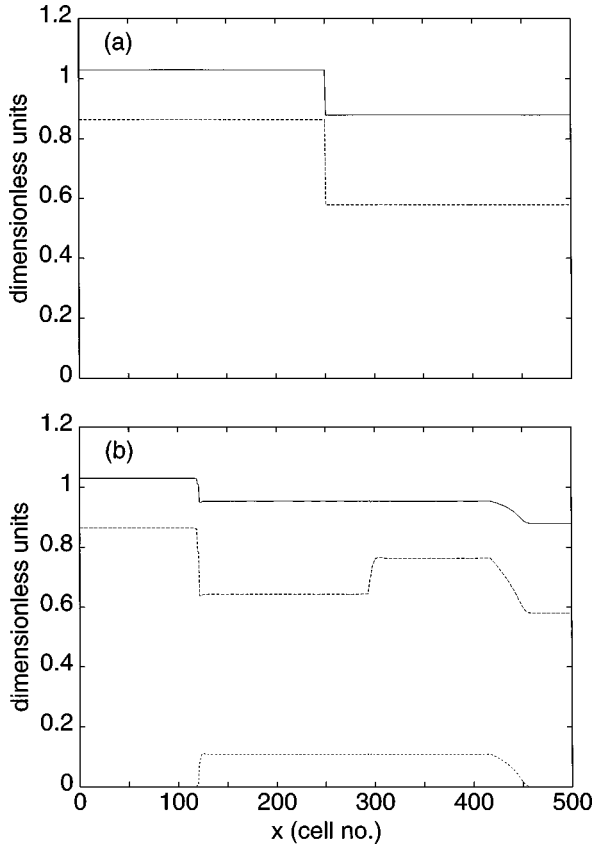

FIG. 3. One-dimensional shock-tube simulation of a van der Waals fluid in an *anomalous* region of the (V,p) plane, with $(V_1,p_1)=(1.7V_0,0.88p_0)$, $(V_2,p_2)=(1.16V_0,1.02p_0)$, and $\mu c_V/R=160/1.986$. Profiles of pressure (solid line), density (dashed line), and velocity (dotted line) are shown at (a) $t=0$;and (b) $t=420$. Note the formation of a leftward-traveling *rarefactive* shock wave in (b) at $x\simeq 120$.

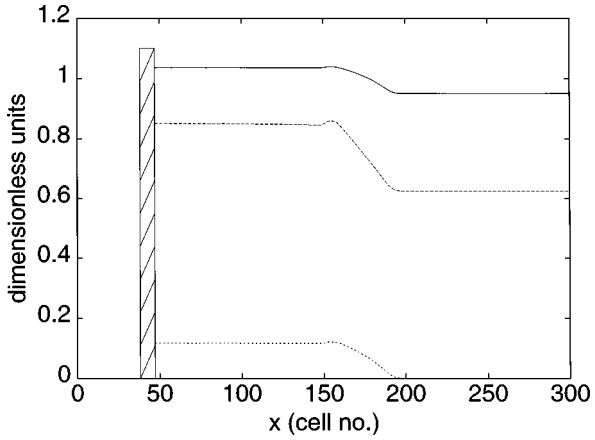

FIG. 4. The piston-launched compressive wave for the initial and final states shown in Fig. 1 at $t=300$ ($\Delta t=0.01$; $\Delta x=1$ initially). The piston moves from rest with an acceleration 0.2 for a time 1.2, after which it travels at a constant subsonic velocity 0.24. In a nonanomalous fluid, this wave would steepen to form a shock, but that is not the case here; as time passes, the profiles of pressure (solid line), density (dashed line), and velocity (dotted line) continue spreading to the right, but never form a shock. The cross-hatched region indicates the location of the piston.

phragm'' in the middle of the tube separates a region of higher pressure and density on the left from a region of lower pressure and density on the right. For $t>0$, this barrier is removed and for nonanomalous fluids, a shock wave propagates into the lower pressure, lower density region, while a rarefactive wave spreads into the higher pressure, higher density region; see Fig. 2(b). For an *anomalous* fluid, however, a very different scenario may occur. Figure 3(b) shows what happens in a run for a van der Waals fluid which evolves from the initial conditions in Fig. 3(a). Here, the upstream and downstream conditions were chosen to make the fluid lie in an anomalous regime (see Fig. 1). In this case, a *rarefactive* shock wave—rather than a compressive one—propagates leftward, while a spreading compressive pulse moves to the right. In all cases, the pressure, density and velocity profiles have been normalized to the values p_0, $\rho_0 \equiv 1/V_0$, and $v_0 \equiv (8a/27b)^{1/2}$, respectively. The speed v_0 can be used to define the ratio of a reference length to a reference time, allowing us to cast the governing equations in dimensionless form before programming them on the computer. For this series of computational runs, the dimensionless spatial and temporal step sizes were $\Delta x=1$ and $\Delta t=0.06$, respectively. For the magnitude of fluid variables occurring in this problem, these values are well within the Courant stability and ''positivity'' requirements for FCT algorithms. Runs performed with even smaller step sizes did not give noticeably different results, indicating that a converged solution had been achieved.

To understand better the dynamical formation of shock waves in the presence of anomalies, as well as to acquire experience with initial conditions which start out as continuous, we conducted a second series of numerical computations in which compressive pulses were launched into quiescent van der Waals fluids by accelerating a piston from rest to a subsonic velocity, then holding it at that velocity. This was accomplished by using a ''sliding rezoning'' mesh in the FCT algorithm. The boundary conditions prescribed at the piston/fluid interface were that the fluid velocity be equal to the instantaneous piston velocity, and that the pressure gradient be equal to the product of the piston acceleration and the local fluid density. (The boundary condition on the density then follows from an adiabatic relation between the pressure and density.) A compressive pulse forms and propagates into the undisturbed medium according to the Riemann simple-wave solution.[12] In a normal medium, this predicts the steepening of the pulse into a compressive shock in a time inversely proportional to the maximum initial spatial gradient of the fluid velocity. However, embedded in the Riemann solution in its usual form is the assumption that $[\rho c(\rho)]'>0$, and when this inequality is reversed, what had been a steepening compressive pulse becomes a spreading one, and a shock refuses to form. In an implosion experiment, shocks are often launched by irradiating one or more faces of the fuel pellet with ionizing radiation which raises the local pressure;[1] this enhanced pressure acts as the ''piston'' for the compressive pulse which then steepens into a shock. In many laser-compression ICF scenarios, it is the expectation that the action of such a piston will launch a compressive pulse which steepens into a shock.

Figure 4 illustrates the complications to the canonical picture of shock wave formation that can arise when a com-

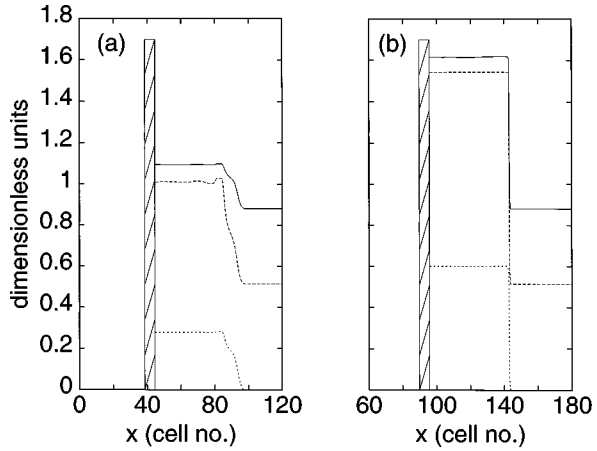

FIG. 5. Piston-launched compressive wave for $(V_1,p_1)=(1.95V_0,0.88p_0)$, which is outside and slightly to the right of the shaded region of Fig. 1. In (a), the piston (initially at rest) moves with an acceleration 0.185 for a time 1.5. The final state $(V_2,p_2)=(1.14V_0,1.07p_0)$ lies just inside the anomalous region, and in this case the compressive wave does not steepen to form a shock. In (b), the piston acceleration has been increased to 0.4; the shock adiabatic still passes through the shaded region of Fig. 1, but the final state $(V_2,p_2)=(0.65V_0,1.62p_0)$ is much higher on this curve, lying outside and to the left of the anomalous region. An ''ideal-gas-like'' shock wave results. Profiles of pressure (solid line), density (dashed line), and velocity (dotted line) are shown at $t=160$, with $\Delta t=0.02$, and $\Delta x=1$ initially.

pressive pulse is launched into an anomalous material. The piston-launched compressive wave connects the initial and final states shown in Fig. 1. Upstream states bear the subscript ''1'' and downstream states the subscript ''2.'' Because both states lie in the anomalous region of the (V,p) plane, though, this wave *does not* steepen to form a shock. Instead, a spreading compressive pulse is the result.

In Figs. 5(a, b), the initial point (V_1,p_1) was chosen to lie outside and slightly to the right of the shaded region of Fig. 1 (with the shock adiabatic still passing through the anomalous region). For final states in or near the left boundary of the anomalous region, shock waves refuse to form [Fig. 5(a)]. As the piston acceleration is increased, though, the final state rides higher along the shock adiabatic, moving further and further to the left of the anomalous region. Eventually, a shock wave does indeed result, and the usual ''ideal-gas-like'' behavior is recovered [Fig. 5(b)].

III. ACOUSTIC EMISSION

In this section, we explore the evolution of perturbed shock fronts by conducting numerical simulations using a two-dimensional FCT-based code. Two different equations of state are considered: (i) a van der Waals fluid with large specific heat; and (ii) an equilibrium dissociation model for diatomic hydrogen. Both simulations are initiated at $t=0$ by first establishing a steady shock propagating in the x-direction with upstream and downstream values of pressure, density and x-component of velocity chosen to be consistent with the Rankine–Hugoniot relations,[5,12] and satisfying the downstream criteria $h_c<h<1+2v_2/c_2$. The planarity of this shock front is then deformed with a single sinusoidal perturbation or ''ripple'' transverse to the direction of motion (the y-direction), and the system is allowed to evolve in time. This perturbation is regarded as ''small'' in the sense that the ratio of its amplitude to wavelength is much less than unity. The boundary conditions in the x-direction are ''inflow'' and ''outflow'' conditions behind and in front of the shock, respectively; periodic boundary conditions are imposed in the y-direction.

For ideal gases, the inequalities $h_c<h<1+2v_2/c_2$ are never satisfied, and acoustic emission from shock fronts cannot occur. Initial perturbations are propagated along the front in the form of running linear waves that decay with time.[30–32] This gives rise to small-amplitude entropy-vortex and sound waves in the downstream wake of the shock.[12] Eventually, the uniformity of the front is restored.

For fluids in which $h_c<h<1+2v_2/c_2$, however, the linear stability analysis of Kontorovich[9] predicts markedly different behavior. In that case, stationary undamped perturbations may exist indefinitely at the shock front.[32] These perturbations may cause the shock to become unstable and emit acoustic waves in the downstream direction—the energy carried away by these emitted waves being drawn from the bulk fluid motion.[12]

Let us now pass to a consideration of each of our model equations of state in turn.

A. Another van der Waals example

Here, we study the stability of two-dimensional shock fronts by once again employing a van der Waals EOS. The first step is to write down expressions for the pressure and specific internal energy:

$$p/p_0=\frac{8(T/T_0)}{3(V/V_0)-1}-\frac{3}{(V/V_0)^2}, \tag{6}$$

$$\varepsilon/\varepsilon_0=\frac{\mu c_V}{R}(T/T_0)-\frac{9}{8(V/V_0)}, \tag{7}$$

where $T_0\equiv 8\mu a/(27Rb)$, and $\varepsilon_0\equiv v_0^2=RT_0/\mu$ are convenient reference values. As in Sec. II, we shall assume that the specific heat is a constant. In order to determine whether a particular shock configuration satisfies the criteria for this class of instabilities, we also need an expression for the adiabatic sound speed, c. Starting from the definition $c^2=(\partial p/\partial\rho)_s$, and using Eq. (A3) in the Appendix, we find

$$c=\frac{3}{2}v_0\left[\left(1+\frac{R}{\mu c_V}\right)\frac{3+(p/p_0)(V/V_0)^2}{6(V/V_0)-2}-\frac{1}{V/V_0}\right]^{1/2}. \tag{8}$$

The ideal gas limit of this expression is obtained by taking $V/V_0\gg 1$, in which case $1+R/\mu c_V\to\gamma$, where $\gamma=c_p/c_V$ is the ratio of specific heats, and c_p is the specific heat at constant pressure. Then, one can easily show that $c=\sqrt{\gamma p/\rho}$, which is the correct expression for the speed of sound in an ideal gas.

With the fundamental shock relation $j=v_1/V_1=v_2/V_2$, Eqs. (6) and (8) can now be used to compute the parameters h and h_c for a van der Waals fluid. Plots of h and h_c, as well as the difference h_c-h, as a function of V_2/V_0 for $V_1/V_0=3.0$, $p_1/p_0=0.66$, and $\mu c_V/R=80$, are shown in Figs. 6(a, b). In Fig. 6(b), it is apparent that a region exists near $V_2/V_0\simeq 0.9$ where the difference h_c-h is indeed nega-

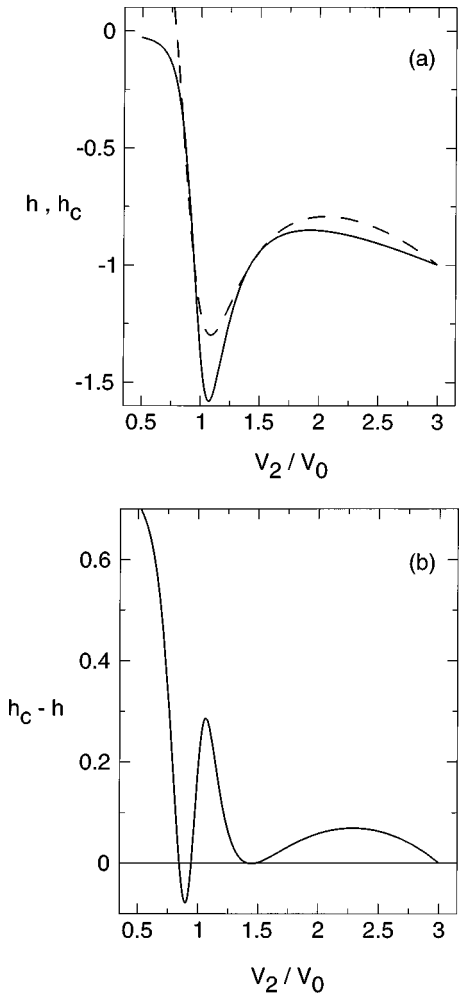

FIG. 6. (a) The plot of h (solid line) and h_c (dashed line) as a function of downstream specific volume V_2/V_0 for a van der Waals fluid with $\mu c_V/R=80$; in (b), the difference h_c-h is shown. The upstream state has $V_1/V_0=3$ and $p_1/p_0=0.88$. Note the region near $V_2/V_0\simeq 0.9$ where the theoretical criteria for acoustic emission instability are satisfied.

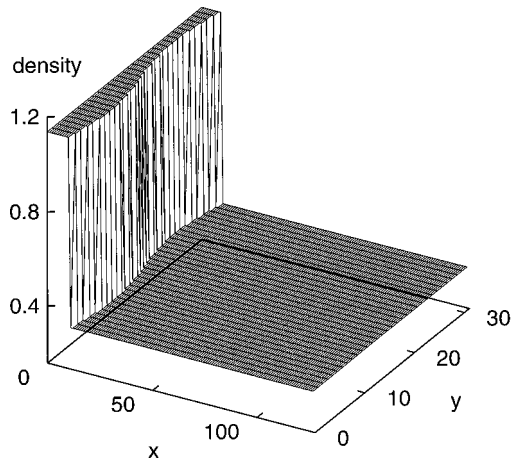

FIG. 7. The surface plot of density in a van der Waals fluid ($\mu c_V/R=80$) showing the perturbed shock front at $t=0$. The upstream and downstream Mach numbers here are $M_1=1.114$ and $M_2=0.744$, respectively.

tive, and hence $h>h_c$ there. Accordingly, we choose $V_2/V_0=0.88$ for the value of our downstream specific volume in our simulation. The associated downstream pressure value in this case is $p_2/p_0=1.068$. The upstream and downstream Mach numbers then have values $M_1=v_1/c_1=1.114$ and $M_2=v_2/c_2=0.744$, respectively.

In Fig. 7, a sinusoidal perturbation has been superimposed on a two-dimensional shock front moving into a quiescent van der Waals fluid on the right; this is taken as the initial condition at time $t=0$ in our simulation. The computational grid is 1024×32 cells with $\Delta x=\Delta y=1$, but in Fig. 7 only the first 128 cells in the x-direction appear. Also note that this figure shows the perturbed density profile, but the pressure and x-component of velocity surfaces (not shown) are deformed with the same sinusoidal ripple; the ratio of perturbation amplitude to wavelength in all cases is 1:8. The y-component of velocity is left unperturbed, and is initially zero everywhere.

Figures 8(a)–(d) show the surfaces of pressure, density, and x- and y-components of velocity, respectively, at time $t=350$. In these plots, the persistence of a perturbation to the shock front is readily discernible, as is the appearance of an acoustic pulse near $x\simeq 200$. What is not so apparent in these figures is the fact that at a very early stage in the calculation, the initial shock has ''split'' into two other shocks. This splitting can be seen more clearly in Figs. 9(a)–(d), which show the double-shock structure at the later time $t=1001$; the acoustic wave is now far downstream from the front, and does not appear in this set of figures. The resulting shocks are now stable. The shock on the right travels slightly faster than the one on the left, so that the distance separating the two increases the longer the simulation is allowed to run. In the region of compressed fluid between the two fronts, perturbations are still visible, but have been almost entirely attenuated by this time. Both shocks possess a uniform planar structure, and will continue propagating to the right indefinitely without overtaking. In this series of computations, the maximum dimensionless time step allowed was $\Delta t=0.005$.

Since the shock splits at such an early stage in the simulation, it is difficult to ascertain whether any numerical evidence of acoustic emission exists, or just what the consequences of satisfying the Kontorovich criteria [Eq. (2)] are, in this example. It is important to realize, though, that the shock splitting observed in Figs. 8 and 9 is almost certainly *not* a result of the conditions $h_c<h<1+2v_2/c_2$ being satisfied. Rather, it is undoubtedly a consequence of the fact that the shock adiabatic for this van der Waals fluid passes through an anomalous region of phase space $[(\partial^2 p/\partial V^2)_s<0]$, a region in which multiple solutions of the Rankine–Hugoniot relations can exist. That is, the initial upstream and downstream states may be connected by either a single shock, or by a pair of successive ones. While a rigorous criterion cannot be given here, it seems reasonable to conclude that shock splitting can happen only if the shock adiabatic curve and the Rayleigh line $j^2=(p_2-p_1)/(V_1-V_2)$ have more than two intersection points, as occurs in this van der Waals example.

We should also remark that the shock splitting observed in these simulations seems to be related to the fact that the shock adiabatic *passes through* a region where $h<-1$ [see

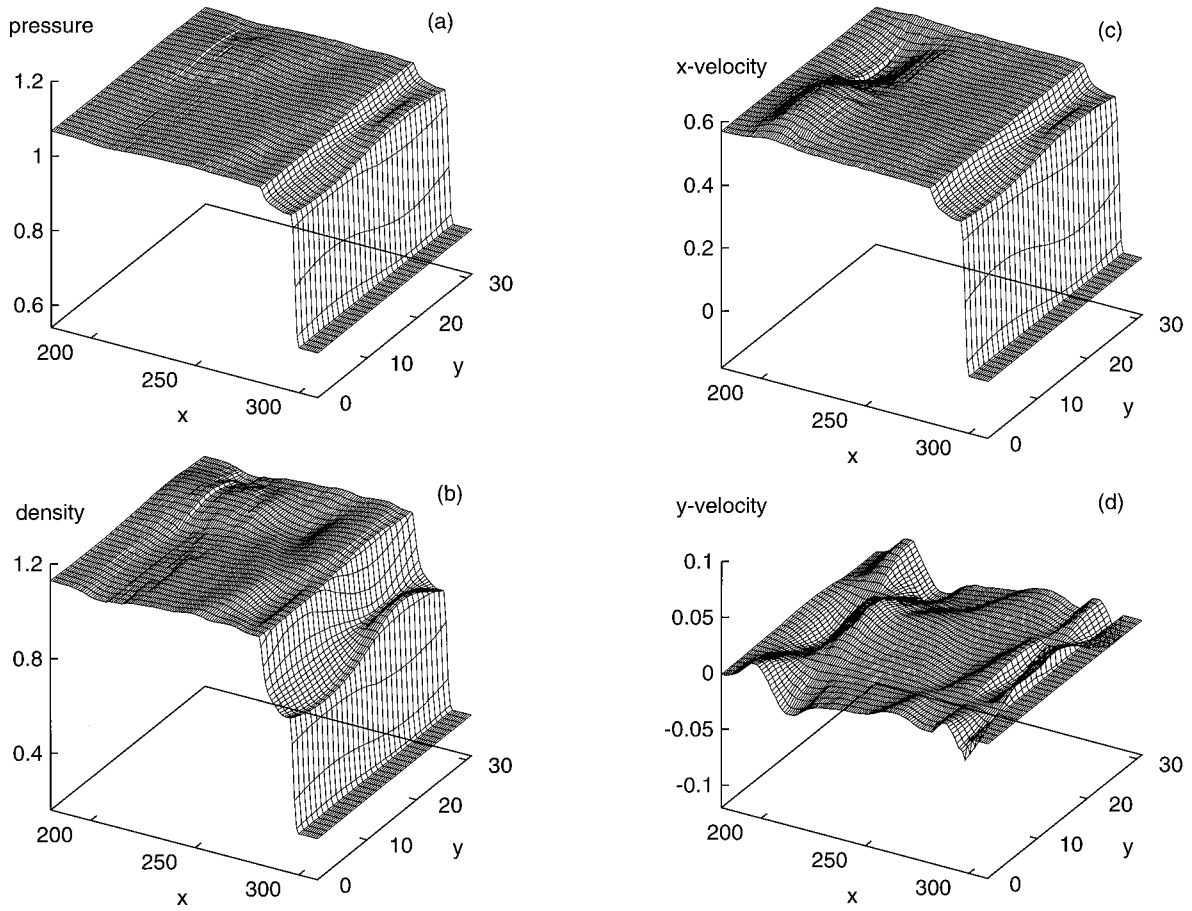

FIG. 8. (a)–(d) Surface plot of perturbed shock (a) pressure, (b) density, (c) x-component of velocity, and (d) y-component of velocity in a van der Waals fluid ($\mu c_V/R=80$) at $t=350$.

Fig. 6(a)], which is one of the limits for the onset of the corrugation instability mentioned earlier.[8,12,21,22] It is well known that in such regions a shock wave may not be ''evolutionary,'' and the solution of the fluid dynamic equations is not necessarily unique.[12,20,22]

For purposes of comparison, Figs. 10(a)–(d) show an analogous run using an ideal-gas EOS with $\gamma=1.4$. The upstream Mach number here is the same as for the van der Waals example: $M_1=1.114$. The initial perturbation amplitude and wavelength are also the same. In this case, though, the perturbation at the front has been attenuated significantly by time $t=280$, and the shock has nearly regained its uniformity. Small-amplitude (sound and entropy-vortex) waves are visible behind the shock, but it is clear that no splitting has occurred.

B. Dissociating hydrogen

In this section we discuss an EOS that is perhaps of greater relevance to ICF research than anomalous van der Waals fluids. Following Zel'dovich and Raizer,[5] we consider an equilibrium dissociation model for diatomic hydrogen, which we briefly outline below. As we shall see, this simple EOS yields a shock adiabatic curve that qualitatively agrees with data of shock-compressed liquid deuterium from recent ICF-related experiments.[4] For additional detail on this model, the reader is referred to pp. 176–188 of Ref. 5.

The expressions for the pressure and specific internal energy density of the dissociating gas are given by

$$p=N(1+\alpha)\rho kT, \tag{9}$$

$$\varepsilon=(1-\alpha)\left(\frac{5}{2}NkT+\varepsilon_\nu\right)+3\alpha NkT+NU\alpha, \tag{10}$$

where ε_ν is the vibrational contribution to the specific internal energy, and U is the dissociation potential (binding energy) of the diatomic molecule. In the case of hydrogen,[33] the dissociation temperature U/k is approximately 5.17×10^4 K. The parameter α is a dimensionless number known as the dissociation fraction, with $0\leqslant\alpha\leqslant1$. Physically, α is the ratio of dissociated molecules to nondissociated ones. Using relations appearing in the Appendix, it is a straightforward exercise to compute the adiabatic sound speed, c, as well as the specific heat at constant volume, $c_V=(\partial\varepsilon/\partial T)_V$, for this model.

By neglecting any interactions between particles, and assuming that the rotational states of the hydrogen molecules are fully excited, even at low temperatures, Zel'dovich and Raizer construct partition functions for both the molecular and atomic hydrogen states. This leads to an expression for the Helmholtz free energy, as a function of the temperature, specific volume, and number of particles for each species of the gas. The authors then obtain the so-called ''law of mass

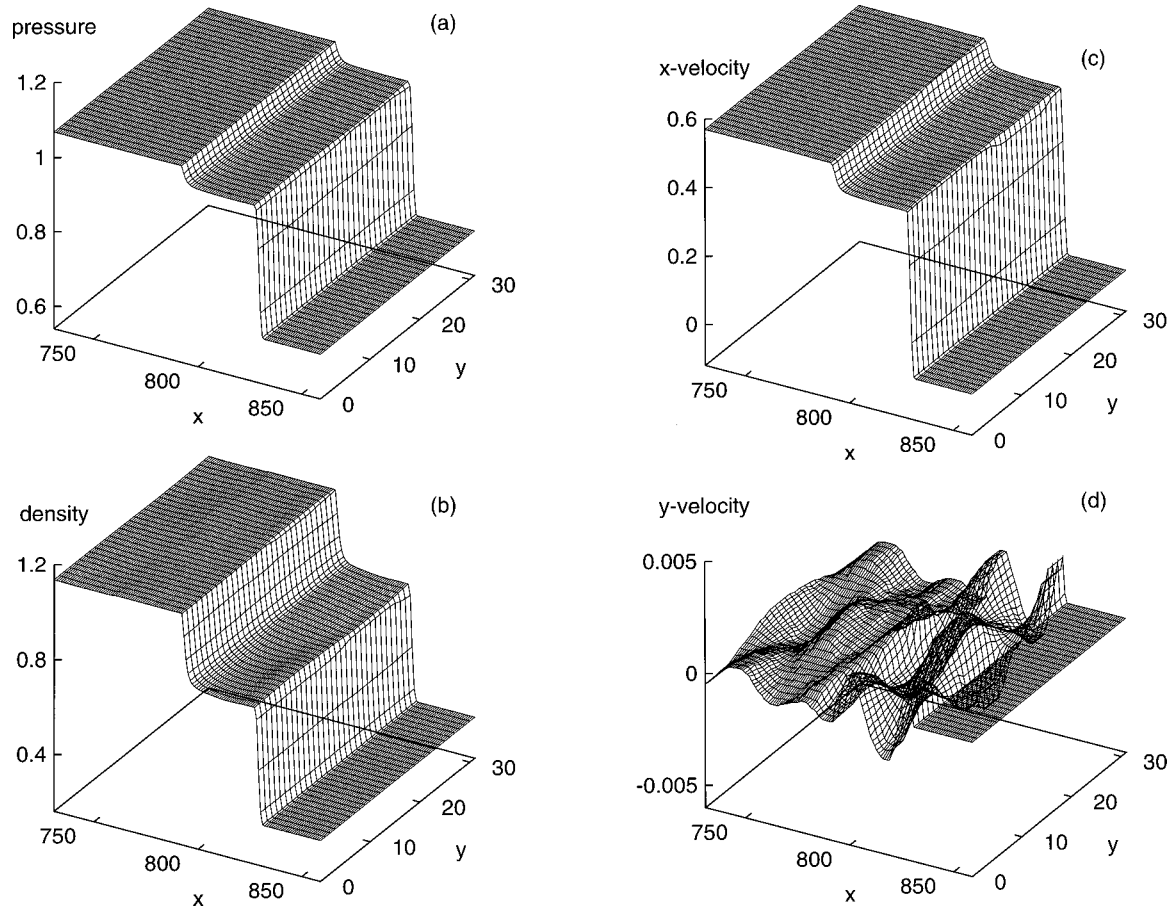

FIG. 9. (a)–(d) The composite shock front of (a) pressure, (b) density, (c) *x*-component of velocity, and (d) *y*-component of velocity in a van der Waals fluid ($\mu c_V/R=80$) at $t=1001$. The splitting of the original shock front is now readily visible. As time passes, the distance between two fronts increases due to their different propagation speeds.

action'' for the dissociative process by using the fact that in thermodynamic equilibrium, the Helmholtz free energy is stationary with respect to the total number of atoms.[34] It should be pointed out that the dissociation process is assumed to take place (and reach a state of equilibrium) infinitely fast, so that no finite-time relaxation effects are considered in this model. The result is an equation relating the dissociation fraction to the density and temperature of the gas:

$$\frac{\alpha^2}{1-\alpha}=\text{const}\times\frac{\sqrt{T}}{\rho Z_\nu}\exp[-U/kT], \tag{11}$$

where the constant on the right hand side contains atomic data specific to hydrogen. In arriving at Eq. (11), it has been assumed that the electronic partition functions contain terms corresponding to only the ground molecular and atomic states. The form of the vibrational partition function, Z_ν, in this equation has yet to be specified. For reasons to be discussed below, we do not necessarily assume, as Zel'dovich and Raizer do, that Z_ν is well described by the high temperature limit of the harmonic-oscillator partition function in which all quantum vibrational energy levels are accessible.

Usually in the derivation of a model EOS for diatomic hydrogen, the vibrational energy levels are approximated by those of a quantum oscillator:[35]

$$\varepsilon_{\nu n}=(n+1/2)h\nu, \quad n=0,1,2,\ldots, \tag{12}$$

where h is Planck's constant and ν is a characteristic vibrational frequency (for hydrogen,[33] $h\nu/k\simeq 6210\,\text{K}$). The vibrational partition function is then found by summing a Boltzmann distribution over all accessible states from $n=0$ to ∞:

$$Z_\nu=\sum_{n=0}^{\infty}\exp\left[-(1/2+n)\frac{h\nu}{kT}\right]$$

$$=e^{-\xi/2}(1+e^{-\xi}+e^{-2\xi}+\cdots)=\frac{e^{-\xi/2}}{1-e^{-\xi}}, \tag{13}$$

where the shorthand notation, $\xi\equiv h\nu/kT$, has been used. The vibrational contribution to the specific internal energy is then given by[34]

$$\varepsilon_\nu=NkT^2\left(\frac{\partial\ln Z_\nu}{\partial T}\right)_V=Nh\nu\left[\frac{1}{2}+\frac{1}{\exp(h\nu/kT)-1}\right], \tag{14}$$

where $Nh\nu/2$ is the so-called ''zero-point energy'' for the oscillator. Note that both Eq. (13) and Eq. (14) are unbounded at high temperatures, both tending to infinity faster

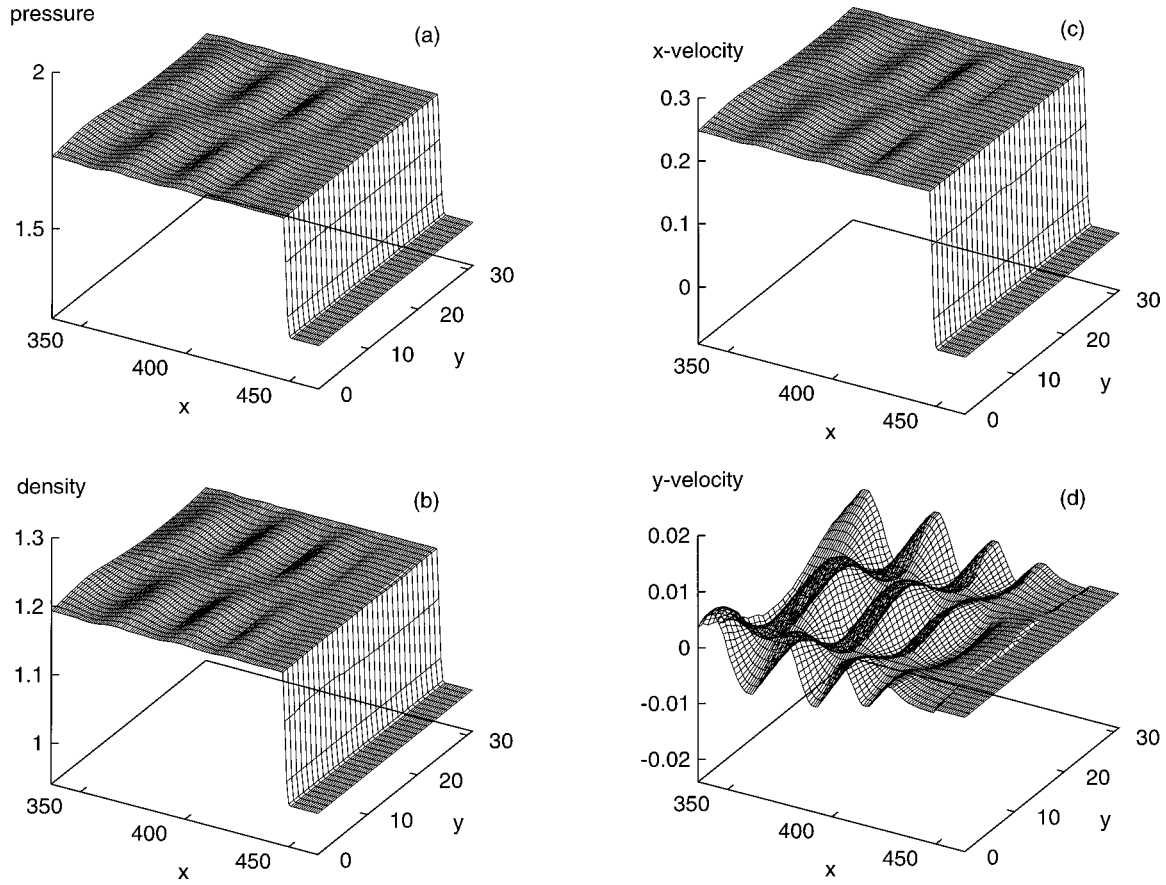

FIG. 10. (a)–(d) Surface plot of perturbed shock (a) pressure, (b) density, (c) x-component of velocity, and (d) y-component of velocity in an ideal gas ($\gamma = 1.4$) at $t = 280$. The upstream Mach number is the same as in the van der Waals example ($M_1 = 1.114$), and, initially, the front was deformed as shown in Fig. 7. Although small-amplitude sound and entropy-vortex waves are visible behind the shock, it is evident that no instability has occurred in this case.

than $\sqrt{T}$ as $T \to \infty$. According to Eq. (11), we then find upon substitution that the dissociation fraction vanishes at high temperatures, which is a nonsensical result.

We can see this point graphically by constructing the shock adiabatic for dissociating hydrogen using Z_ν as written in Eq. (13). Figure 11 shows such an adiabatic for the upstream state $\rho_1 = 0.17\,\mathrm{g/cm^3}$ and $T_1 = 20\,\mathrm{K}$, values which were chosen to mimic realistically a typical initial state of cryogenic ICF targets. The adiabatic curve is parametrized by the value of the downstream temperature, T_2. A plot showing the corresponding value of the downstream dissociation fraction α along this curve also appears in the figure. The downward-pointing arrow indicates that the curve for α should be read on the horizontal axis, but without units. At low temperatures, we see that $\alpha = 0$. As the temperature is increased, α departs from zero, but does not monotonically approach the value 1 as we would expect from physical considerations. Instead, α experiences a maximum value of about 0.5, then begins to decrease again, eventually going to zero as $T \to \infty$. The same general behavior is obtained if one ''assumes the vibrational states are fully excited,'' as Zel'dovich and Raizer do, and replaces Z_ν with its high-temperature limit, $kT/h\nu$.

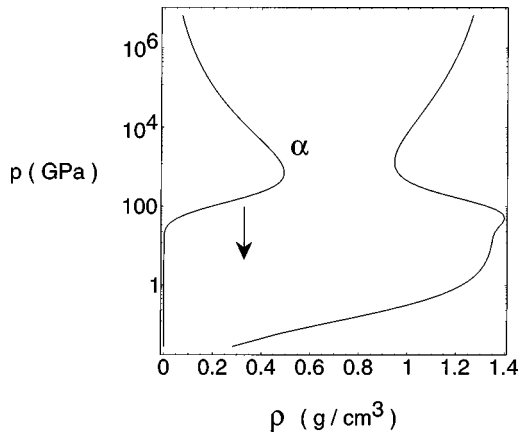

FIG. 11. Shock adiabatic for dissociating hydrogen. The form of the vibrational partition function used to generate this curve was $Z_\nu = e^{\xi/2}(1 - e^{-\xi})^{-1}$, where $\xi \equiv h\nu/kT$, which leads to an unphysical high-temperature behavior of the dissociation fraction α. The initial data for the upstream state were $\rho_1 = 0.17\,\mathrm{g/cm^3}$ and $T_1 = 20\,\mathrm{K}$. The downward pointing arrow indicates that α should be read on the horizontal axis, but without units.

This unsatisfactory feature of α is ameliorated by a vibrational partition function that remains finite as $T \to \infty$. Equation (13) can be modified to have this property (and thus yield a dissociation fraction that goes to unity at high temperatures) by taking the upper limit in the summation to be a finite integer, rather than infinity. Such a restriction is seen to make sense on physical grounds for the following reasons. As it stands, Eq. (13) is meant to represent a sum

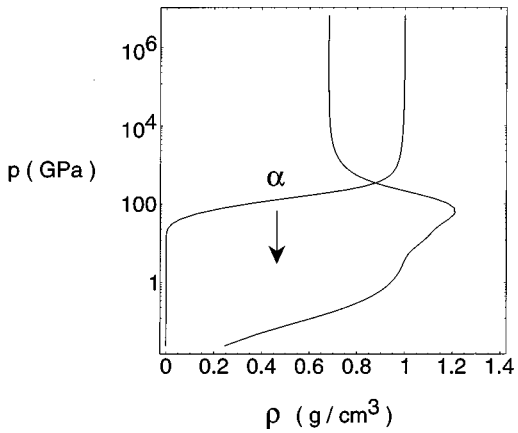

FIG. 12. The improved shock adiabatic for dissociating hydrogen. Using the first two terms in the series for the vibrational partition function, $Z_\nu = e^{\xi/2}(1+e^{-\xi}+\cdots)$, where $\xi \equiv h\nu/kT$, leads to a dissociation fraction α that now has the correct high-temperature behavior. Keeping any finite number of terms in the series yields the same qualitative result. The upstream data are the same as used in Fig. 11.

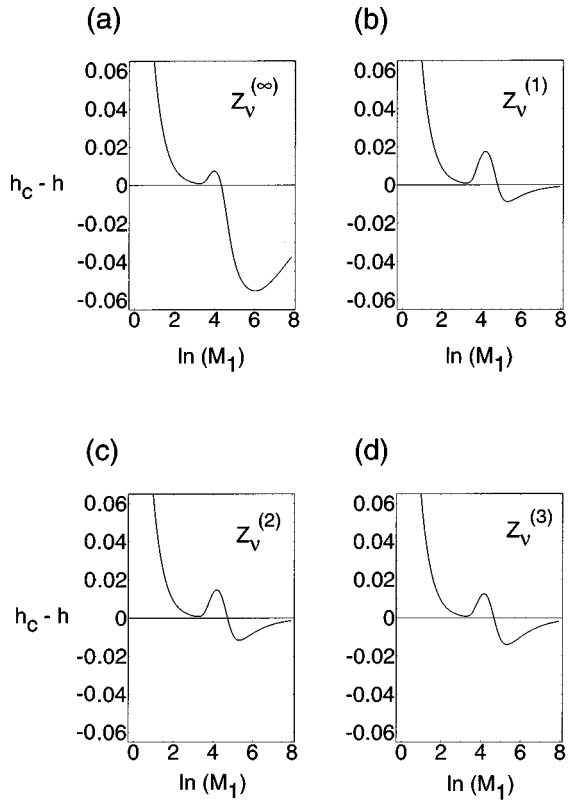

FIG. 13. (a)–(d) Plots of the difference $h_c - h$ vs upstream Mach number for dissociating H_2 and various partial sums of the vibrational partition function $Z_\nu^{(N)}$. In all cases, the upstream data are the same as in Figs. 11 and 12.

over all vibrational energy levels that are *accessible* to a diatomic molecule. As the temperature is raised, though, a given molecule will eventually dissociate; thus, only a finite number of these states can be realized, which places a finite upper bound on the series in Eq. (13). (Note that a more rigorous treatment using the so-called ''Morse'' potential[36] for an anharmonic oscillator adopts a similar restriction.) In the present analysis, just how many terms should appear in the summation for Z_ν is not clear. We only note here that since diatomic hydrogen has a characteristic vibrational temperature, $h\nu/k$, that is approximately 12% of the dissociation temperature, U/k, it seems appropriate to us that at most the first ''several'' terms should be used. Figure 12 shows a shock adiabatic curve drawn for the same initial data as in Fig. 11, but using just the first two terms in the series for the vibrational partition function. More terms can be included, but as long as the total number is finite, the same qualitative behavior results (of course, quantitative features such as the location and extent of the ''nose'' of the adiabatic curve will be affected by this choice). We now find that at high temperatures, $\alpha \to 1$, which is commensurate with our physical intuition, and a much more satisfactory asymptotic behavior.

The equilibrium dissociating model for diatomic hydrogen outlined above, while crude, is a useful place to begin studying the phenomenon of acoustic emission instabilities in ICF compression scenarios. As in the van der Waals example, this EOS admits a range of shock strengths over which the theoretical criteria for instability are satisfied. Unlike the van der Waals case, though, it never fulfills the condition for anomalous behavior. That is not to say, though, that the occurrence of anomalous effects in real ICF target materials can be necessarily ruled out. After all, ICF pellets usually have an inhomogeneous composition, and the passage of shock waves through substances other than DT has to be considered. Moreover, additional phase changes—which are often the harbingers of anomalous activity—are expected to occur in DT at very high temperatures where the present dissociative EOS certainly does not provide a complete description of the shock dynamics. Examples of such high-temperature phase changes may include ionization and a transition to a metallic state.[3]

For the present EOS model, it turns out that the range of shock strengths (upstream Mach numbers) for acoustic emission to occur in theory is only slightly affected by the number of terms included in the series for the vibrational partition function, Z_ν. Figure 13 shows plots of the difference $h_c - h$ as a function of the upstream Mach number M_1 for four different partial sums $Z_\nu^{(\mathrm{N})}$, where N denotes the number of vibrational energy levels included beyond the zero-point energy. In these plots, the initial state was again chosen to be typical of the density and temperature of cryogenic ICF targets prior to shock compression: $\rho_1 = 0.17\ \mathrm{g/cm^3}$ and $T_1 = 20\ \mathrm{K}$. The notation $Z_\nu^{(\infty)}$ refers to the case in which every vibrational energy level is permitted, as in Eq. (13). We see that in all four cases, there is a critical shock strength of about $M_1 \sim e^{4.5} \sim 90$ beyond which h always exceeds h_c, and the criteria for instability are met. The value of this critical Mach number is dependent on the parameters of the upstream state, and of course would be different if the gas were initially at ''room temperature,'' or if multiple-stage shock compressions were used.

In an effort to simulate dynamically the emission of sound from two-dimensional shocks with this model EOS, a series of computational runs similar to those performed for the van der Waals fluid was conducted using an FCT-based code. The numerical approach for this system, though, was slightly more complicated than in the ideal gas or van der

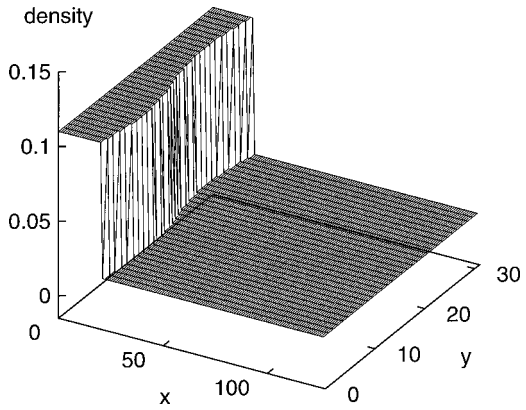

FIG. 14. The density surface plot of the perturbed shock front ($M_1 \simeq 150$) in the dissociating hydrogen-gas model at $t=0$. The upstream and downstream states have densities and temperatures $\rho_1 = 0.17\ \mathrm{g/cm^3}, T_1 = 20\ \mathrm{K}$, and $\rho_2 = 0.98\ \mathrm{g/cm^3}, T_2 = 7.97\times 10^4\ \mathrm{K}$, respectively. In this computation, densities and temperatures were cast in dimensionless form using the reference values $\rho_0 = 8.89\ \mathrm{g/cm^3}$ and $T_0 = 5.24\times 10^4\ \mathrm{K}$. According to the linear theory, the downstream state satisfies the criteria for acoustic emission instability. There, the dissociation fraction α is 0.49.

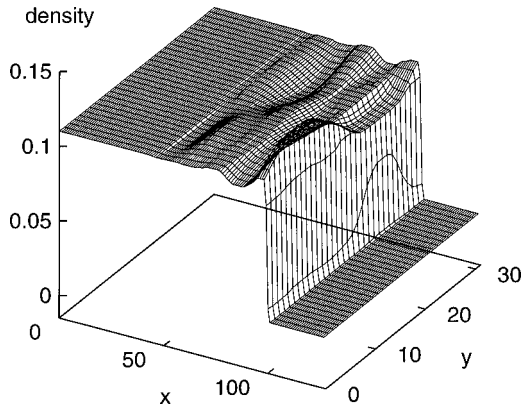

FIG. 15. The density surface plot of the shock front in the dissociating hydrogen–gas model at $t=20$. At this early time in the simulation, the occurrence of an instability is uncertain.

Waals cases because of the inability to algebraically express ε as a simple function of ρ and p *only* [see Eqs. (9)–(11)]. Starting from specified initial conditions, the FCT algorithm solves the 2D Euler equations in conservative form to give new values of ρ, $\mathbf{v}$, and ε, but before the next time step can begin, updated values of α and T (and hence p) must also be determined. In the code, this was accomplished through the use of a Newton–Raphson root-finding procedure.[37]

In order to maximize the likelihood of witnessing this phenomenon numerically, we chose the vibrational partition function for which the difference $h_c - h$ was most pronounced, i.e., $Z_\nu^{(\infty)}$. As discussed above, such a choice becomes unphysical at high-enough temperatures where the dissociation fraction does not monotonically approach unity. For lower-temperature downstream states lying near the ''tip of the nose'' on the shock adiabatic curve, though, this choice can be made without introducing any spurious features in the shock dynamics. For our first simulation, we chose a downstream state characterized by $\rho_2 = 0.98\ \mathrm{g/cm^3}$ and $T_2 = 7.97\times 10^4\ \mathrm{K}$. This corresponds to an upstream Mach number $M_1 \simeq 140$ and a value $h_c - h \simeq -0.04$ in Fig. 13(a).

As before, a planar shock front was perturbed at time $t=0$ with a single sinusoidal ''ripple.'' Figure 14 shows the initial density profile in which this perturbation is readily apparent. (In this figure, the density values are nondimensionalized with respect to a reference value $\rho_0 = 8.89\ \mathrm{g/cm^3}$.) Although not shown, the shock fronts in pressure and x-component of velocity were distorted in exactly the same way, with the amplitude-to-wavelength ratio taken once again to be 1:8. The value of the y-component of fluid velocity was initially zero everywhere.

Figures 15 and 16 show the density at two subsequent times, $t=20$ and $t=50$, respectively. Due to the larger sound and propagation speeds, the time step in this series of simulations was necessarily smaller than in the van der Waals example; here, the maximum allowed value of Δt was 5×10^{-4}. Not surprisingly, it is apparent that also unlike the van der Waals case, the perturbation has not ''triggered'' a splitting of the shock wave since $(\partial^2 p/\partial V^2)_s$ is nowhere negative in this example. Sound and entropy-vortex waves are visible in the downstream wake of the shock, but evidently no instability has occurred. The behavior appears to be essentially that of an ideal gas, despite the fact that the theoretical criteria for acoustic emission instability ($h_c < h < 1 + 2\,v_2/c_2$) are met. Using sinusoidal perturbations of other amplitudes and wavelengths, this simulation was repeated for a higher upstream Mach number of $M_1 \simeq 400$, which for $Z_\nu^{(\infty)}$, corresponds to $h_c - h \simeq -0.058$—the absolute minimum of the curve in Fig. 13(a). Once again, though, the initial perturbation was attenuated with no clear indication that an instability had taken place.

We should also mention that subsequent computer runs were performed using other methods of perturbing the shock front. In particular, small Gaussian ''bumps'' were superimposed on the downstream flow field behind a uniform planar shock in an effort to stimulate unstable emission activity. Although these Gaussian perturbations featured a wider

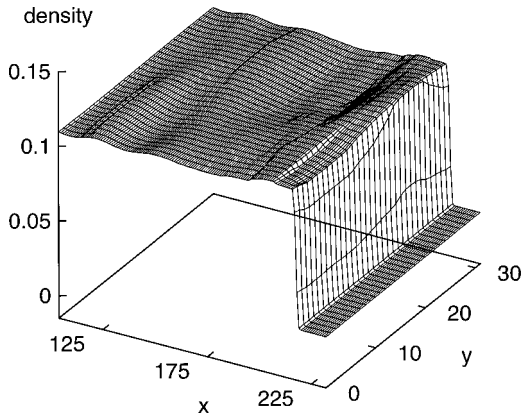

FIG. 16. The density surface plot of the shock front in the dissociating hydrogen–gas model at later time ($t=50$). The initial perturbation is significantly diminished and has left sound and entropy-vortex waves in the downstream flow. Despite the fact that the theoretical criteria for instability have been satisfied in this example, no clear evidence is apparent in the simulation. The behavior resembles that of an ideal gas.

spectrum of perturbing wave vectors than the sinusoidal deformation, they too failed to precipitate any unmistakable numerical evidence of acoustic emission phenomenon in the dissociating hydrogen gas example.

IV. DISCUSSION AND CONCLUSIONS

The equations of state of materials used in shock-imploded ICF targets are far from well-known. In typical compression scenarios, these targets experience enormous pressure and temperature changes, often spanning several orders of magnitude. In the process, it is likely that a variety of phase changes such as melting, vaporization, molecular dissociation, ionization, and possibly even a transition to a metallic state,[3] are crucial physical considerations in understanding the physics of the shock compression. The extent to which such nonideal effects complicate shock behavior and the efficiency of the compression, though, has not been well elucidated. Here, we have attempted to take a few tentative steps towards addressing these issues by conducting numerical studies of two peculiar shock-wave phenomena that possibly play a role in ICF compression schemes. They are (i) anomalous behavior, and (ii) acoustic emission instabilities. Neither phenomenon occurs in an ideal gas.

We have seen that shock wave formation and stability in a van der Waals fluid, with a large heat capacity and in the vicinity of a liquid–gas phase transition, can be greatly affected by shock adiabatic curves that pass through anomalous regions of the (V,p) plane—regions where the adiabatic sound speed is a rapidly decreasing function of the density and $(\partial^2 p/\partial V^2)_s$ is negative. In such cases, compressive pulses may not steepen to form shocks, if their intended initial and final states lie in or close to anomalous regions. Whether or not shocks form is a subtle question of where those states lie, relative to those regions. Additionally, we have observed that a compressive planar shock, once formed, is not necessarily a stable and unique solution of the hydrodynamic equations; in the two-dimensional case, perturbations may precipitate a splitting of the shock in two, with each resulting shock wave propagating with a different velocity. In our simulations, this split was accompanied by the generation of a downstream acoustic pulse whose direction of propagation was opposite to that of the original shock. The extent to which a converging geometry (e.g., spherical) modifies any of these findings is unclear at present, and will require further investigation. While theoretical expressions for the EOS of high-density ICF-target materials that could be used in a dynamical code may still be lacking, there is every reason to expect the van der Waals EOS to exemplify typical anomalous behavior.

Additional study also will be required to ascertain how considerations such as boundary conditions and perturbation amplitude and wavelength affect shock stability. Particular quantitative issues that may be of interest include the prediction of when splitting occurs, and the strength of the resulting shocks. Subsequent calculations using the van der Waals EOS have revealed that a perturbation amplitude-to-wavelength ratio of 1:16 can also ''trigger'' a two-dimensional shock front to split, but the amplitudes and propagation velocities of the resulting shocks are different than those appearing in Figs. 8 and 9, where initially this ratio was 1:8. For smaller ratios, though, clear evidence of shock splitting is not always seen in the simulations, suggesting that there may be a threshold for this phenomenon.

The second exotic shock mechanism considered (acoustic emission) is a class of shock instabilities that can occur when the parameter $h=j^2(dV/dp)_H$ (where the derivative is taken along the shock adiabatic and evaluated at the downstream state) exceeds a critical value, h_c, which depends on the downstream Mach number and the compression ratio. Previous theoretical analyses[9,10,12] predict that perturbations to a shock front can stimulate the continuous emission of acoustic waves from the downstream face of the shock. This instability has apparently been observed for some time in shock-tube experiments,[24,25] in which weak perturbations of the shock front can ostensibly arise from fluid inhomogeneities and/or surface irregularities on the walls of the apparatus.

Although a simple dissociative EOS for diatomic hydrogen gas also was shown to fulfill the theoretical criteria for instability, no clear evidence of acoustic emission was observed during the associated dynamical simulations. It is possible that this result is to some extent tied up with the particular features of the numerical approach employed. It is also possible that the theoretical analysis of shock wave stability based on a linearization of the gas-dynamic equations does not yield complete or accurate criteria for emission in all circumstances. Kuznetsov,[20] for instance, has argued that the normal mode representation of perturbations used in the linear theory gives only an indirect indication of the nonstationary character of the flow, and does not provide a correct description of its long-term development. The results of our investigation seem to be in accord with this latter assertion, suggesting that additional work may be needed to more clearly elucidate our theoretical understanding of shock wave instability.

Quite likely, though, the reason that an acoustic emission instability was not observed in our simulations has to do with the perturbation method employed. The sinusoidal deformation of the front, while convenient and simple to implement numerically, is probably not an optimal means of stimulating acoustic emission activity. As Fowles[10] has pointed out, acoustic emission from an unstable shock front can be viewed as a resonant reflection phenomenon. That is, for acoustic waves impinging on the downstream face of the shock, a range of incident angles exists such that the amplitude of the reflected waves exceeds that of the incident waves. In particular, there is a *certain* angle of incidence where the ratio of reflected to incident amplitudes becomes infinite. To see more clearly (stimulated) acoustic emission phenomena in a numerical experiment, then, it is probably necessary to superimpose on the downstream flow field a perturbation of the form $\exp(-i\omega t+ik_x x+ik_y y)$, where ω, k_x, and k_y are the angular frequency and wavenumbers in the x- and y-directions, respectively, of an acoustic wave. These parameters would be chosen to make the propagation direction (angle of incidence) of the wave lie in the narrow band of resonant reflection. In a dynamical code, though,

such an arrangement presents significant challenges. One can no longer just seek solutions of the 2D Euler equations from initial data. Most likely, it would be necessary to include a term in the governing differential equations that represents a ''source'' of monochromatic plane waves propagating in a fixed direction with a wave vector $\mathbf{k}=k_x\hat{\mathbf{x}}+k_y\hat{\mathbf{y}}$. At present, it is not entirely clear how this would be accomplished. Efforts to stimulate acoustic emission from a two-dimensional shock front using an initial Gaussian perturbation (which contains a wide spectrum of $\mathbf{k}$ vectors) of the downstream flow field did not provide any additional insight into this mechanism.

Besides van der Waals fluids and dissociating hydrogen gases, a third ICF-relevant EOS was identified during the course of this investigation that also met the criteria for acoustic emission. This was an ionization model for very strong shocks in monatomic hydrogen. It should be pointed out that at the downstream parameters of interest in this study (e.g., $\rho_2=0.98\,\mathrm{g/cm^3}$ and $T_2=7.97\times10^4\,\mathrm{K}$), effects due to ionization cannot rightfully be ignored, as energy losses due to dissociation and ionization are approaching the same order of magnitude. Due to our inability to successfully witness an instability in the dissociating hydrogen gas example, though, a series of numerical simulations was not conducted for this EOS. Salient details are discussed on pp. 192–201 of Ref. 5, where the ionization fraction is determined from a Saha equilibrium. Note, however, that unlike the stability analysis of ionizing shocks in argon given by Mond and Rutkevich,[23] satisfaction of the condition $h_c<h<1+2\,v_2/c_2$ here does not depend on any finite relaxation-time effects.

Undoubtedly, though, shock stability is sensitively linked with nonequilibrium effects in fluids such as the retarded excitation of some degrees of freedom.[5,23] While the dissociative EOS model used in this paper was an equilibrium one—which assumed that the dissociation reaction of a given hydrogen molecule proceeded infinitely fast so that no relaxation mechanisms were taken into account — it may be profitable in the future to include nonequilibrium dissociation (by permitting finite relaxation time scales in the computational model), and study its effect on the formation of instabilities in shocks.

The immediate practical consequences of anomalous behavior, shock splitting, and acoustic emission instability for ICF research is unclear and will require time and experience to determine. In addition, diagnosing the presence of these phenomena in actual ICF targets is probably exceedingly difficult at present. It is clear, though, that the temporal profile of driver mechanisms (*e.g.*, lasers in the case of ''direct drive'') is sensitively linked to the expectation that a compressive pulse will steepen into a shock of a particular strength at a particular time. High compression may be impaired—and successful ignition spoiled—if such a shock does not form or splits into a composite wave structure before reaching the DT fuel at the core of an ICF pellet. It seems to us that the use of cladding materials is some pellet designs (such as tangles of complex hydrocarbon fibers with large heat capacities) may add to the likelihood of this occurrence.

ACKNOWLEDGMENTS

This work was supported in part by the U.S. Naval Research Laboratory under Grant No. N000014-96-1-G005. The authors wish to thank Professor John Winn and Professor Michael Sturge for useful discussions, and for supplying the coexistence curve data appearing in Fig. 1. Useful comments by two anonymous referees are also acknowledged.

APPENDIX: USEFUL THERMODYNAMIC RELATIONS

In order to determine whether a particular shock wave configuration satisfies the criteria for acoustic emission, the parameter h must be computed from the shock adiabatic curve. Since EOS data is most often specified with the specific volume and temperature taken as the preferred independent variables, e.g., $p=p(V,T)$, a particularly convenient means of calculating the ordinary differential equation for the shock adiabatic is provided by the following relation among derivatives of thermodynamic quantities:[21]

$$\left(\frac{dp}{dV}\right)_H=\frac{(\partial p/\partial V)_s+(\frac{1}{2})\,(p-p_1)\Gamma/V}{1-(\frac{1}{2})\,(V_1-V)\Gamma/V}, \tag{A1}$$

where the total derivative on the left hand side is taken along the shock adiabatic and evaluated at the downstream state; the parameter Γ is the so-called ''Grüneisen'' index,

$$\Gamma=\frac{V}{c_V}\left(\frac{\partial p}{\partial T}\right)_V, \tag{A2}$$

and

$$\left(\frac{\partial p}{\partial V}\right)_s=\left(\frac{\partial p}{\partial V}\right)_T-\frac{T}{c_V}\left(\frac{\partial p}{\partial T}\right)_V^2. \tag{A3}$$

In the study of anomalous shock wave properties, it is also useful to have an expression for the second partial derivative of p with respect to V at constant s. We find

$$\begin{aligned}\left(\frac{\partial^2 p}{\partial V^2}\right)_s=&\left(\frac{\partial^2 p}{\partial V^2}\right)_T-\frac{3T}{c_V}\left(\frac{\partial p}{\partial T}\right)_V\frac{\partial^2 p}{\partial V\partial T}\\&+\frac{3T}{{c_V}^2}\left(\frac{\partial p}{\partial T}\right)_V^2\left(\frac{\partial c_V}{\partial V}\right)_T\\&+\frac{T}{{c_V}^2}\left(\frac{\partial p}{\partial T}\right)_V^3\left[1-\frac{T}{c_V}\left(\frac{\partial c_V}{\partial T}\right)_V\right],\end{aligned} \tag{A4}$$

which agrees with formulas given by Bethe[6] and Thompson.[15]

[1] J. D. Lindl, ''Development of the indirect-drive approach to inertial confinement fusion and the target physics basis for ignition and gain,'' Phys. Plasmas **2**, 3933 (1995).
[2] R. M. More, K. H. Warren, D. A. Young, and G. B. Zimmerman, ''A new quotidian equation of state (QEOS) for hot dense matter,'' Phys. Fluids **31**, 3059 (1988).
[3] N. C. Holmes, M. Ross, and W. J. Nellis, ''Temperature measurements

and dissociation of shock-compressed liquid deuterium and hydrogen,'' Phys. Rev. B **52**, 15 835 (1995).
[4]L. B. Da Silva, P. Celliers, G. W. Collins, K. S. Budil, N. C. Holmes, T. W. Barbee, Jr., B. A. Hammel, J. D. Kilkenny, R. J. Wallace, M. Ross, R. Cauble, A. Ng, and G. Chiu, ''Absolute equation of state measurements on shocked liquid deuterium up to 200 GPa (2 Mbar),'' Phys. Rev. Lett. **78**, 483 (1997).
[5]Y. B. Zel'dovich and Y. P. Raizer, *Physics of Shock Waves and High-Temperature Hydrodynamic Phenomena* (Academic, New York, 1966), Vol. I, II.
[6]H. A. Bethe, ''The theory of shock waves for an arbitrary equation of state,'' Office of Scientific Research and Development Report OSRD No. 545, 1942 (unpublished).
[7]R. G. McQueen, in *High Pressure Equations of State: Theory and Applications*, edited by S. Eliezer and R. A. Ricci (North-Holland, Amsterdam, 1991), pp. 101–216.
[8]S. P. D'yakov, ''On the stability of shock waves,'' Zh. Éksp. Teor. Fiz. **27**, 288 (1954) (Translation into English: Air Force Office of Scientific Research Report AFOSR-TN-56-406, 1956).
[9]Z. M. Kontorovich, ''Concerning the stability of shock waves,'' Zh. Éksp. Teor. Fiz. **33**, 1525 (1957) [Sov. Phys. JETP **6**, 1179 (1957)].
[10]G. R. Fowles, ''Stimulated and spontaneous emission of acoustic waves from shock fronts,'' Phys. Fluids **24**, 220 (1981).
[11]P. G. Fowles and A. F. P. Houwing, ''Instabilities of shock and detonation waves,'' Phys. Fluids **27**, 1982 (1984).
[12]L. D. Landau and E. M. Lifshitz, *Fluid Mechanics*, 2nd ed. (Pergamon, Oxford, 1987).
[13]A. C. Ivanov and S. A. Novikov, ''Rarefactive shock waves in iron and steel,'' Zh. Éksp. Teor. Fiz. **40**, 1880 (1961) [Sov. Phys. JETP **13**, 1321 (1961)].
[14]P. A. Thompson, ''A fundamental derivative in gas dynamics,'' Phys. Fluids **14**, 1843 (1971).
[15]P. A. Thompson and K. C. Lambrakis, ''Negative shock waves,'' J. Fluid Mech. **60**, 187 (1973).
[16]P. A. Thompson and Y. G. Kim, ''Direct observation of shock splitting in a vapor-liquid system,'' Phys. Fluids **26**, 3211 (1983).
[17]P. A. Thompson, G. C. Carfano, and Y. G. Kim, ''Shock waves and phase changes in a large-heat-capacity fluid emerging from a tube,'' J. Fluid Mech. **166**, 57 (1986).
[18]R. Courant and K. O. Friedrichs, *Supersonic Flow and Shock Waves* (Wiley, New York, 1974).
[19]R. Menikoff and B. J. Plohr, ''The Riemann problem for fluid flow of real materials,'' Rev. Mod. Phys. **61**, 75 (1989).
[20]N. M. Kuznetsov, ''Contribution to shock-wave stability theory,'' Zh. Éksp. Teor. Fiz. **88**, 470 (1985) [Sov. Phys. JETP **61**, 275 (1985)].
[21]G. W. Swan and G. R. Fowles, ''Shock wave stability,'' Phys. Fluids **18**, 28 (1975).
[22]C. Gardner, ''Comments on 'Stability of step shocks,' '' Phys. Fluids **6**, 1366 (1963).
[23]M. Mond and I. M. Rutkevich, ''Spontaneous acoustic emission from strong ionizing shocks,'' J. Fluid Mech. **275**, 121 (1994).
[24]R. W. Griffiths, R. J. Sandeman, and H. G. Hornung, ''The stability of shock waves in ionizing and dissociating gases,'' J. Phys. D **9**, 1681 (1976).
[25]I. I. Glass and W. S. Liu, ''Effects of hydrogen impurities on shock structure and stability in ionizing monatomic gases. Part I. Argon,'' J. Fluid Mech. **84**, 55 (1978).
[26]J. P. Boris and D. L. Book, ''Flux-corrected transport. I. SHASTA, A fluid transport algorithm that works,'' J. Comput. Phys. **11**, 38 (1973).
[27]D. L. Book, J. P. Boris, and K. Hain, ''Flux-corrected transport II: Generalizations of the method,'' J. Comput. Phys. **18**, 248 (1975).
[28]J. Boris, A. Landsberg, E. Oran, and J. Gardner, ''LCPFCT—A Flux-corrected transport algorithm for solving generalized continuity equations,'' Naval Research Laboratory Report No. NRL/MR/6410-93-7192, 1993 (unpublished).
[29]C. Kittel and H. Kroemer, *Thermal Physics*, 2nd ed. (Freeman, New York, 1980), pp. 287–294.
[30]N. C. Freeman, ''On the stability of plane shock waves,'' J. Fluid Mech. **2**, 397 (1957).
[31]W. K. van Moorhem and A. R. George, ''On the stability of plane shocks,'' J. Fluid Mech. **68**, 97 (1975).
[32]M. A. Liberman and A. L. Velikovich, *Physics of Shock Waves in Gases and Plasmas* (Springer-Verlag, Berlin, 1986).
[33]S. Eliezer, A. Ghatak, H. Hora, and E. Teller, *An Introduction to Equations of State: Theory and Applications* (Cambridge University Press, Cambridge, 1986), p. 43.
[34]K. Huang, *Statistical Mechanics*, 2nd ed. (Wiley, New York, 1987).
[35]A. Beiser, *Concepts of Modern Physics* (McGraw-Hill, New York, 1981).
[36]H. Haken and H. C. Wolf, *Molecular Physics and Elements of Quantum Chemistry* (Springer-Verlag, Berlin, 1995), pp. 149–155.
[37]W. H. Press, B. P. Flannery, S. A. Teukolsky, and W. T. Vetterling, *Numerical Recipes: The Art of Scientific Computing* (Cambridge University Press, Cambridge, 1987), pp. 254–259.